Circulating Tumor Cell Phenotyping via High-Throughput Acoustic Separation

Mengxi Wu, Po-Hsun Huang, Rui Zhang, Zhangming Mao, Chuyi Chen, Gabor Kemeny, Peng Li, Adrian V. Lee, Rekha Gyanchandani, Andrew J. Armstrong, Ming Dao,* Subra Suresh, and Tony Jun Huang*

The study of circulating tumor cells (CTCs) offers pathways to develop new diagnostic and prognostic biomarkers that benefit cancer treatments. In order to fully exploit and interpret the information provided by CTCs, the development of a platform is reported that integrates acoustics and microfluidics to isolate rare CTCs from peripheral blood in high throughput while preserving their structural, biological, and functional integrity. Cancer cells are first isolated from leukocytes with a throughput of 7.5 mL h^{-1}, achieving a recovery rate of at least 86% while maintaining the cells' ability to proliferate. High-throughput acoustic separation enables statistical analysis of isolated CTCs from prostate cancer patients to be performed to determine their size distribution and phenotypic heterogeneity for a range of biomarkers, including the visualization of CTCs with a loss of expression for the prostate specific membrane antigen. The method also enables the isolation of even rarer, but clinically important, CTC clusters.

1. Introduction

Circulating tumor cells (CTCs) have been extensively investigated over the past several decades through a variety of techniques.[1] Expanding effort in this area has been catalyzed by the notion that CTCs can be used within the framework of minimally invasive diagnostic and therapeutic assessments—in the context of "liquid biopsy"—to provide valuable guidance for cancer therapy.[2–11] Furthermore, CTCs can reveal important information about tumor heterogeneity and genetic mutations that initiate cancer's metastatic and drug resistance mechanisms.[12–16] However, efforts aimed at the capture and analysis of CTCs to elucidate the mechanisms of cancer development or to improve clinical outcomes have yet to realize their full potential. This lack of progress is in part due to the disruptive nature of the collection process, the relative paucity of viable cells following collection, and the rarity of such cells in the circulatory system. CTCs are extremely rare in peripheral blood (usually 0–100 cells per mL), and more robust methods to optimize their separation and collection for downstream analysis are needed.[17,18] Therefore, rapid, biocompatible, and highly accurate cell separation methods are required to capture a range of CTC phenotypes without altering cell properties and viability.

Early CTC separation methods focused on using tumor-specific antibodies to capture cancer cells on magnetic particles or other solid surfaces.[18–23] While these methods have demonstrated successful isolation of CTCs, the selection of antibodies generates an inherent bias toward a subgroup of cancer cells. In order to improve CTC isolation techniques, many complementary separation strategies have been developed.

Dr. M. Wu, Dr. P.-H. Huang, C. Chen, Prof. T. J. Huang
Department of Mechanical Engineering and Material Science
Duke University
Durham, NC 27708, USA
E-mail: tony.huang@duke.edu

R. Zhang, Dr. Z. Mao
Department of Engineering Science and Mechanics
The Pennsylvania State University
University Park, PA 16802, USA

G. Kemeny, Prof. A. J. Armstrong
Duke Cancer Institute and Departments of Medicine
Surgery, and Pharmacology and Cancer Biology
Duke University Medical Center
Durham, NC 27710, USA

The ORCID identification number(s) for the author(s) of this article can be found under https://doi.org/10.1002/smll.201801131.

DOI: 10.1002/smll.201801131

Prof. P. Li
Eugene Bennett Department of Chemistry
West Virginia University
Morgantown, WV 26506, USA

Prof. A. V. Lee, Dr. R. Gyanchandani
Department of Pharmacology & Chemical Biology
Magee-Women's Research Institute
UPMC Hillman Cancer Center
University of Pittsburgh
Pittsburgh, PA 15213, USA

Prof. M. Dao
Department of Materials Science and Engineering
Massachusetts Institute of Technology
Cambridge, MA 02139, USA
E-mail: mingdao@mit.edu

Prof. S. Suresh
Nanyang Technological University
50 Nanyang Avenue, Main Campus, Singapore 639798, Singapore

One approach entails "negative selection" that isolates CTCs using anti-CD45, anti-CD66b, and magnetic beads to remove white blood cells (WBCs).[24] By removing WBCs and red blood cells (RBCs), the concentration of CTCs is greatly enhanced in the final solution. The device achieved 3.8-log depletion of WBCs, and could process 8 mL of blood in 2 h. Despite the high removal rate of blood cells, the use of a micropillar array for RBCs removal makes the device more prone to channel clogging. Inertia-based cell separation has also been applied. This method involves a spiral microfluidic chip that achieves up to 4-log depletion of WBCs with a throughput of 3 mL h^{−1}.[25] By adding a step to facilitate the lysis of RBCs, the device's speed was further increased to 7.5 mL in 40 min.[26] However, the high flow rate requirements of inertial separation could exert large shear stresses on the cancer cells, thereby decreasing their proliferation afterwards. Dielectrophoresis (DEP) is another label-free separation method that exploits the electrical property differences between cancer cells and normal cells.[27,28] However, the low conductive medium and the high electrical field strength required for DEP could compromise the integrity of separated cells.

We recently reported an acoustic-based CTC separation platform capable of isolating CTCs from peripheral blood samples obtained from cancer patients.[29] Among existing CTC separation methods, acoustic-based approaches have advantages such as simplicity, cost-effectiveness, and versatility. More importantly, they separate cells in a label-free, contactless, and biocompatible manner, and offer the possibility to preserve cell integrity and functions. Acoustics-based separation methods operate at a power intensity and frequency similar to ultrasonic imaging, which has been proven safe on human tissue and cells.[29–32] Moreover, they require neither a change in medium nor the labeling of cells with external markers. Unlike mechanical centrifugation[25] or filtration techniques, they do not subject the cells to severe forces that could alter their gene expression, mechanical characteristics, and physiological status. As a result, CTCs isolated by acoustic methods are more likely to be maintained in their native states for subsequent culturing and follow-up analysis. The throughput (≈1.2 mL h^{−1}) of earlier experiments involving the acoustic CTC separation method, however, limits widespread adoption, since there is a need for clinical CTC assays that can process a tube of blood (≈7.5 ml) in about 1 h or less, rather than the duration of about 6–8 h needed using current technology. Several scientific and technical advances are needed to improve throughput of the acoustic CTC separation method for the following reasons. First, high separation throughput facilitates the retrieval of a sufficient number of patient-derived cancer cells from a large volume of peripheral blood in a relatively short time, making it more suitable for clinical applications. Second, shortening the processing time of acoustics-based separation would help preserve cell freshness, viability, and integrity, and maximize the potential to establish in vitro cultured CTC lines. Third, it makes it possible to perform tasks that were not possible with previous studies, such as investigating CTC phenotypic and biomarker heterogeneity or isolating CTC clusters that may otherwise be lost with slower processing methods due to CTC degradation.

In this work, we first introduce and validate a new device design that enables up to a sevenfold improvement in the
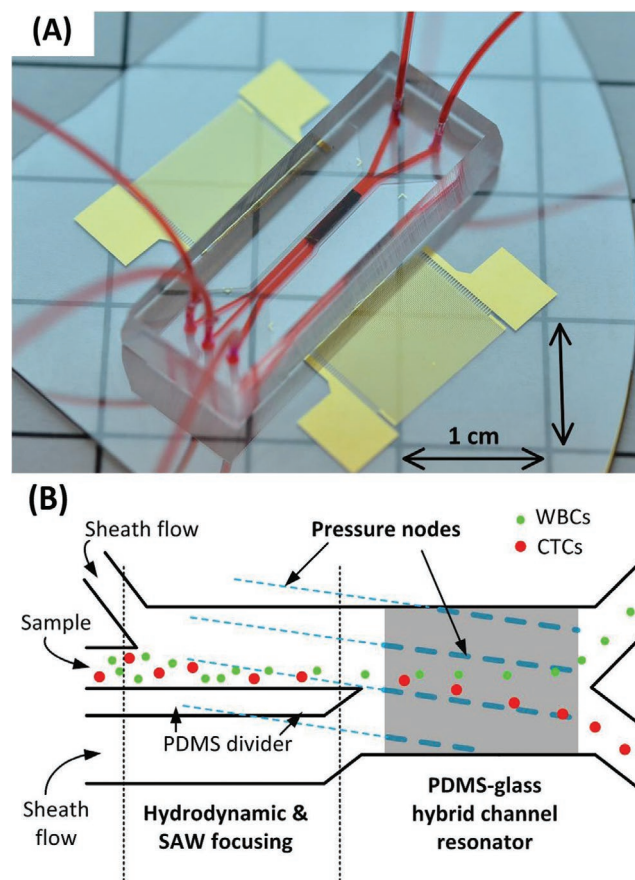

Figure 1. Working principle and structure of the high-throughput acoustic CTC separation devices. A) Photo showing the size of the acoustic CTC separation device with respect to the scale of a 1 × 1 cm grid. The embedded glass layer is painted black to make it visible upon insertion. B) Schematic of the microchannel as viewed from the top. Cells were injected from the central inlet and focused along the PDMS divider. In the hybrid PDMS–glass channel resonating area, CTCs (red dots) and WBCs (green dots) are separated because of the difference in the lateral shift.

throughput of the acoustic separation method. The starting point for this work is our acoustic CTC separation device (**Figure 1**), which uses tilted-angle standing surface acoustic waves.[29] In order to improve the throughput, we employed a poly(dimethylsiloxane) (PDMS)–glass hybrid channel to form an acoustic enclosure, thereby increasing the energy density and the resulting throughput. In addition to the hybrid channel, we introduced a divider into the device configuration (Figure 1B). The local decrease in cell velocity induced by PDMS divider improves CTC separation efficiency and specificity due to the longer travel time for the cell within the acoustic field. We tested and validated the performance of this approach by testing a mixture of leukocytes spiked with cancer cells. The separation throughput was increased to 7.5 mL h^{−1}. While operating at this improved throughput level, the separation efficiency of rare cancer cells from WBCs was maintained. We then applied this technique to study clinical samples and successfully separated CTCs from blood samples collected from patients with metastatic prostate cancer. This was followed by detailed characterization of the phenotypic heterogeneity of prostate CTCs by biomarkers such as prostate specific

membrane antigen (PSMA) and size/clustering. These studies suggest that the method shown here for isolating CTCs has the potential for high-throughput isolation of viable CTCs sufficient for downstream molecular and phenotypic analyses to further enable the practice of precision medicine in oncology.

2. Results

2.1. Hybrid PDMS–Glass Resonator Design to Improve Separation Throughput

The acoustic CTC separation device is schematically shown in Figure 1A. A PDMS microfluidic channel is bonded to a piezoelectric substrate between a pair of interdigitated transducers (IDTs). When radio frequency voltage signals are applied, IDTs generate two Rayleigh waves travelling in opposite directions which interfere within the microfluidic channel. Thus, a standing wave field is formed where periodic wave nodes and antinodes are generated. Cells flowing through these periodic pressure nodes and antinodes are subjected to different acoustic radiation forces, resulting in lateral displacement. The acoustic radiation forces are linearly related to the acoustic energy density.[29–34] To enhance the acoustic energy density within the microchannel and to improve the throughput of the acoustic separation device, we employed a PDMS–glass hybrid channel to form an acoustic enclosure. In particular, we embedded a thin glass layer (130 µm in thickness) at the top of the microchannel (**Figure 2**). Glass has a much larger acoustic impedance (≈12 MPa s m^{-1}) than PDMS (0.98 MPa s m^{-1}) and water (≈1.49 MPa s m^{-1}). Thus, whereas only 4% of the acoustic energy is reflected back to the channel in the PDMS channel used in our previous design,[29] the reflected acoustic energy is increased to 89% in the new hybrid PDMS–glass channel (Note 1 and Figure S1, Supporting Information).

Numerical simulation (Figure 2C) of the acoustic energy density distribution in a cross-section of the microchannel shows that the hybrid channel design has a higher acoustic energy density than the PDMS channel used in acoustic separation devices. With the higher acoustic energy density, the device generates larger acoustic radiation forces on cells as they flow through, thereby enabling higher separation throughput.

2.2. Divider Design to Modify Fluid Velocity Profile and to Improve Separation Accuracy

In order to further improve the separation efficiency while maintaining high throughput, we modified the channel configuration by introducing a PDMS divider at the junction of the inlets (Figure 1B). **Figure 3** shows the ability of the PDMS divider to adjust fluid velocity profiles in the microchannel. For a simple straight channel, the velocity profile in the cross-section maintains a parabolic distribution: at the channel walls, the velocity of the fluid is zero. The velocity increases toward the center of the channel and reaches a maximum at the center.[35] In previous work, the cell solution was infused from the central inlet so that the cells would be focused in the center of the channel (as indicated by the arrows), where the velocity is maximum. In the new design, a PDMS divider is located in the center of the modified channel creating two additional boundary layers besides those from the channel walls; the downstream flow profile changes accordingly. As a result, a shadow-like, low-velocity region forms and spans the acoustic field (Figure 3A). In this case, cells are focused near the PDMS divider and their flow is retarded due to viscous forces. The cells continue traveling slowly as they enter the active acoustic region. Figure 3B shows the velocity distribution of a straight channel (black parabolic curve) compared against the velocity distribution at various positions along the modified channel. At a distance of 0.5 mm after the channel convergence, the fluid
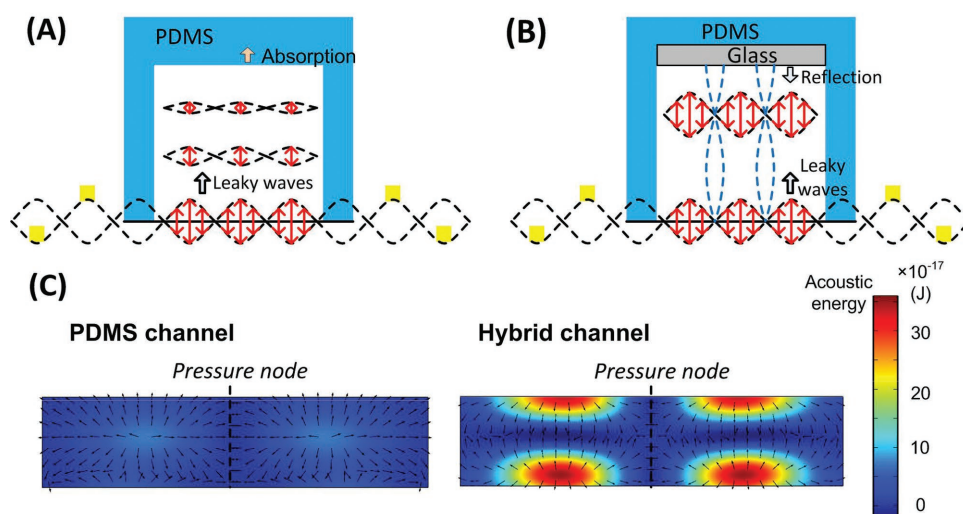

Figure 2. Schematic illustrations and corresponding numerical simulations of a PDMS/glass hybrid channel as an acoustic enclosure. A,B) Cross-sections of the PDMS channel used in our previous acoustic separation devices (A) and a PDMS–glass hybrid channel used in this work (B) illustrate the effect of a hard material such as glass in conserving acoustic energy. C) Numerical simulation of acoustic energy density in the PDMS and hybrid channels. The side-view cross-sections show that the hybrid channel has a higher acoustic energy density because of the formation of an acoustic enclosure.
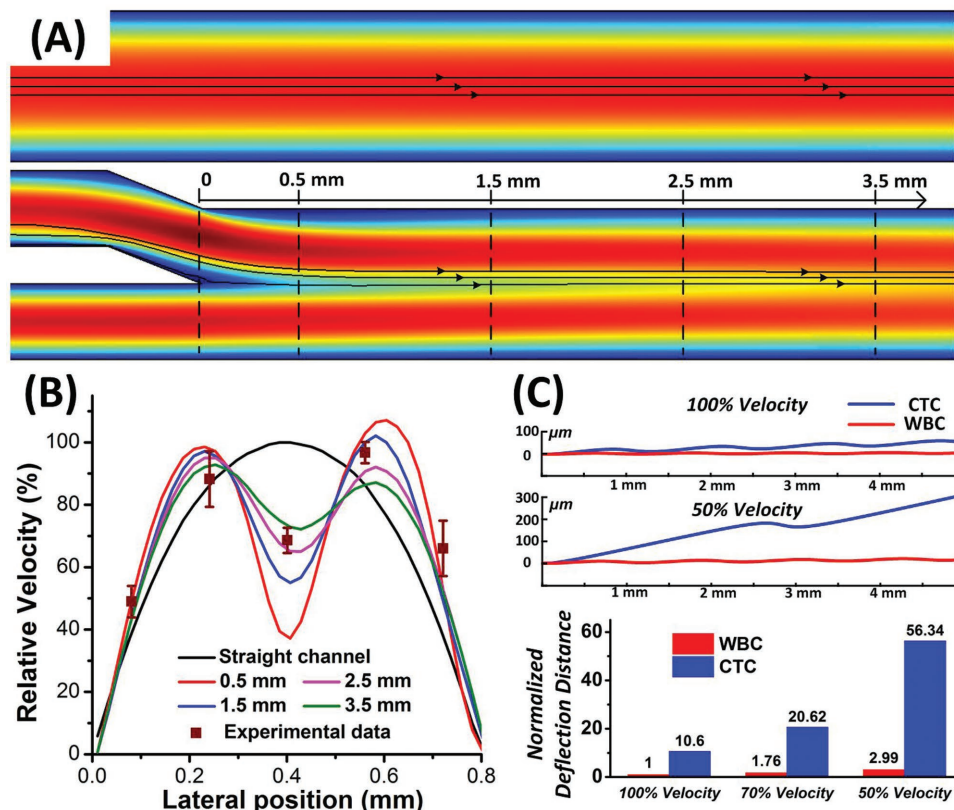
Figure 3. Numerical simulation of the velocity distribution in the modified channel with a divider and its effectiveness at increasing separation efficiency. A) Top view of the velocity distributions in the conventional channel (top) and the modified channel with a divider (bottom). The arrows indicate positions of cells flowing in either channel with blue areas indicating low velocity and red areas indicating high velocity. B) Velocity distribution curves across the channels show that in the modified channel, a low-velocity region was created in the center after the PDMS divider. The velocity profiles in planes at 0.5, 1.5, 2.5, and 3.5 mm, with respect to the flow direction, after the PDMS divider are graphed. Experimental data show the average velocity of cells in different region. C) The lateral deflection displacements of CTCs and WBCs were impacted by cell velocity. A slower velocity increased the cells' displacement.

velocity is reduced by ≈60% in the center as compared to that of the straight channel. Even 3.5 mm away from the PDMS divider, the velocity profile is still reduced by more than 20%. The simulation is supported by experimental data, which indicate a significant drop in velocity at the center of the channel. The experimental results were obtained by recording particle trajectories and calculating the velocities of 50 individual particles distributed throughout each region.

The velocity shadow successfully decreased the speed of the cells as they entered the acoustic field zone, enabling more time for the acoustic radiation force to differentiate CTCs from WBCs. The resulting lateral displacement induced by acoustic field is thus enhanced when compared to the straight channel design. Figure 3C shows a numerical simulation of cell deflection as a function of flow velocity. The trajectories of the CTCs and WBCs are simulated under the conditions of 100% and 50% of the maximum velocity in a straight channel. From the trajectories, the decrease in velocity leads to a larger lateral shift and as such, CTCs can be separated from WBCs more efficiently. We then calculated the lateral deflection distance of the CTCs and WBCs under different velocities. For WBCs, the distance increases 1.76 and 2.99 times, respectively, when the velocities are 70% and 50%, respectively, when compared

against the situation that the velocity of cells equates to the maximum velocity in a straight channel. As for CTCs at 50% velocity, the shift is 5.3 times greater than at 100% velocity. The difference in the lateral deflection between CTCs and WBCs, which increases from 10 to 18.8 times, is noteworthy. Thus, by implementing this divider design, we have improved the overall lateral displacement of CTCs and markedly enhanced the separation efficiency.

2.3. Acoustic Separation of Cancer Cells from White Blood Cells

To test the effectiveness of the two innovations (hybrid PDMS–glass resonator and divider) in improving separation throughput and accuracy, we used the separation devices to isolate PC-3, LnCaP, HeLa, and MCF-7 cancer cells, which represent a range of hormone-sensitive prostate cancer cells, castration-resistant prostate cancer cells, cervical cancer cultured cell lines, and breast cancer cultured cell lines, respectively. WBCs were collected from 1 mL of blood from healthy volunteers and then resuspended with cancer cells stained with Calcein-AM in phosphate-buffered saline (PBS). In order to improve visualization of the separation process, a large number of cancer
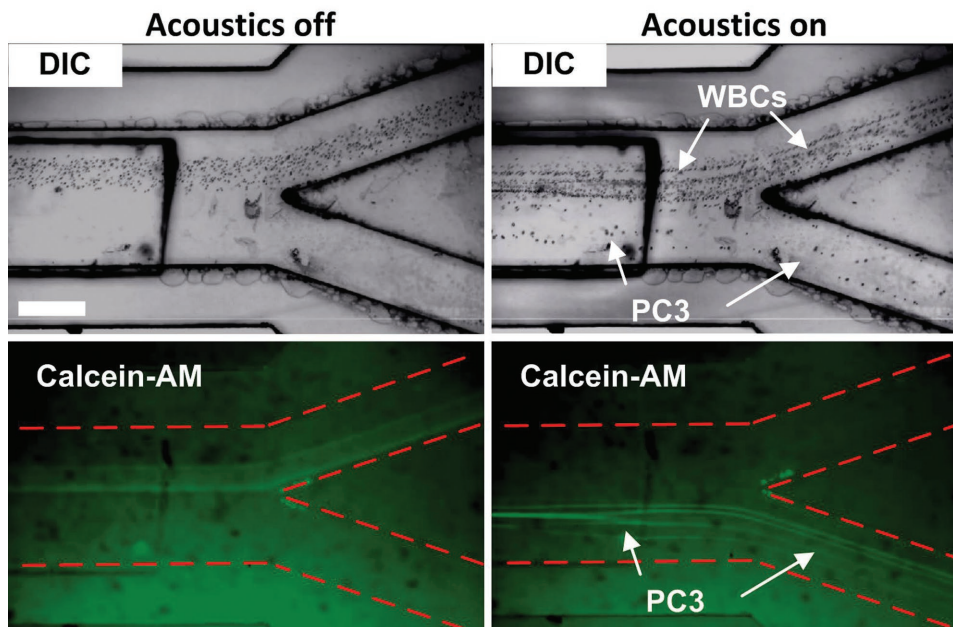
ADVANCED
SCIENCE NEWS
www.advancedsciencenews.com

NANO · MICRO
small
www.small-journal.com

Figure 4. High-throughput acoustic separation of cancer cells from WBCs. PC3 cells are stained by Calcein-AM and spiked into a 1 mL suspension of WBCs. All the cells flow into the top waste outlet when the acoustic field is not activated. After the acoustic field is activated, PC3 cells are pushed toward the bottom collection outlet while the majority of the WBCs continue flowing to the waste outlet. Scale bar: 400 μm.

cells are mixed with this suspension. The ratio of cancer cells to WBCs varied from 1:5 to 1:10. Cell separation at the outlet region is recorded under fluoresence microscopes, as shown in **Figure 4** and Figures S2–S4 (Supporting Information). Cells were focused in the center of the channel. The flow rate of the cell stream was 7.5 mL h^{-1}, and the flow rates of the two sheath flows were 6.6 and 13.2 mL h^{-1}, respectively. When the acoustic field was not activated, cells were not deflected and all flowed toward the waste outlet. Once the acoustic field was activated, there was a clear separation between cancer cells and healthy WBCs. Cancer cells, which are stained with green fluorescence, were deflected by the acoustic field and directed toward the collection outlet (Figure S5, Supporting Information), whereas the majority of WBCs remained in the waste outlet. This experimentally demonstrates that our acoustic separation platform can separate cancer cells from WBCs at a flow rate of 7.5 mL h^{-1}.

Next, we performed an isolation process that modeled rare cancer cells in whole blood. The rare cell population was simulated by incorporating 50 to 1000 Calcein-AM-stained cancer cells into 1 mL of WBCs. The concentration of WBCs ranged from 3 to 6 million cells per mL. This mixture was processed through the acoustic separation device at a flow rate of 7.5 mL h^{-1}. Cells were gathered from both the collection and waste outlets. The fluorescent cancer cells were counted at both outlets, and the recovery rate was calculated by dividing the number of cancer cells in the collection outlet by the total number of cancer cells from both outlets. An average recovery rate greater than 86% is obtained for all these samples.

In order to verify if our new separation device preserves cell integrity, we conducted long-term cell culture of PC-3 and LnCaP cells, following acoustic separation. The flow rate and input power were the same as those used in the cell separation experiments above. Cells collected from the collection outlet

were cultured in an incubator and were monitored. The morphology of the separated cancer cells appeared to be consistent with those in the literature.[18–27] They started to attach to the Petri dish after 12 h and proliferated every 2 d (Figure S6, Supporting Information), suggesting that the cells recovered after sorting and proliferated at a rate similar to that before sorting.

2.4. Acoustic Separation of CTCs from Blood Samples from Prostate Cancer Patients

After demonstrating cancer cell separation with blood samples that contained predetermined proportions of cancer cells from cultures, we performed CTC separation using blood samples that were collected from patients with prostate cancer. Men with castration-resistant metastatic prostate cancer and widespread bone metastases were enrolled as part of an IRB-approved clinical protocol at Duke University under informed consent, and blood samples were collected for CTC isolation. All men were receiving radium-223 therapy as part of their standard therapy, and all had received prior hormonal therapies for metastatic prostate cancer. Details of the eligibility criteria are provided on clinicaltrials.gov under NCT02204943. Immunostaining of cytokeratin 8, 18(CK8, 18), and pan-leukocyte marker CD45 as well as nucleus staining of 4′,6-diamidino-2-phenylindole (DAPI) were used to identify the cells. CTCs were identified as CK8,18+/CD45−/DAPI+; DAPI− was regarded as debris or dust; cells were otherwise identified as WBCs (Figure S7, Supporting Information).

Figure 5 and Figure S8 (Supporting Information) show typical immunostaining patterns of isolated CTCs. Based on the immunostaining criteria, we have identified CTCs from five clinical blood samples, with counts ranging from 0.93 to
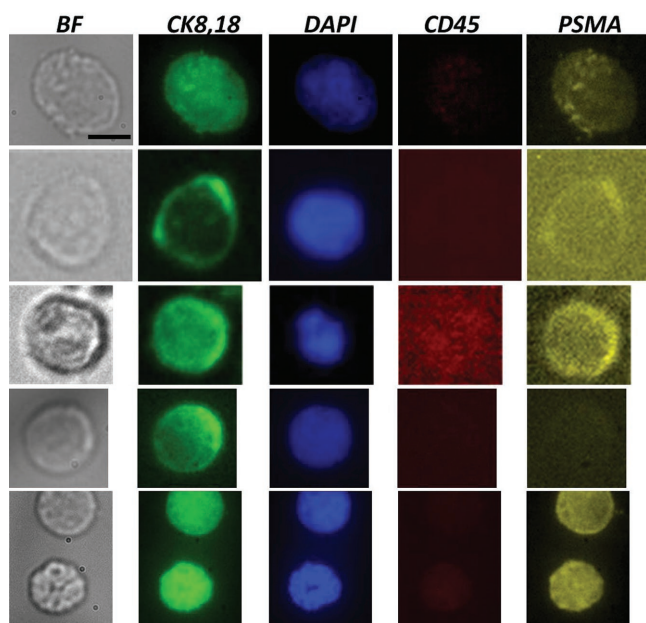
**ADVANCED
SCIENCE NEWS**

www.advancedsciencenews.com

NANO · MICRO

small

www.small-journal.com

Figure 5. Acoustic isolation of CTCs from the blood sample of a single patient with castration-resistant, bone-metastatic prostate cancer. Typical images of the immunostaining pattern for individual CTCs. BF: bright field images. Cells are identified by the cytokeratin marker CK8,18 and the pan-leukocyte marker CD45. DAPI is used to stain the cell nucleus. The immunostaining pattern for CTCs is positive when CK8,18+/DAPI+/CD45−. The PSMA expression level varies, showing the heterogeneity of CTCs. Scale bar: 10 µm.

400 CTCs per mL (**Figure 6**). We also examined the expression of the PSMA, which is a transmembrane protein that has considerable overexpression on most prostate cancer cells, and thus is used as a diagnostic imaging target and has emerged as a potential therapeutic target.[36–39] We examined PSMA expression in CTCs. It is notable that although the majority of prostate cancer CTCs had PSMA overexpression, a fraction of the CTCs expressed relatively low levels of PSMA (Figures 5 and 6A). Loss of PSMA positivity in the CTCs from prostate cancer patients could be a reflection of tumor heterogeneity and suppression of androgen receptor activity during

castration-resistant progression.[40] This result also indicates that PSMA-targeted imaging and directed therapies could miss some of the tumor cells and therefore be ineffective.

We also characterized the size distribution of CTCs and WBCs. The diameters of 70 CTCs and 64 WBCs were measured and are plotted in Figure 6B. The diameter of CTCs has a median diameter of 16.5 µm with a 95% confidence interval at 0.61 µm. Furthermore, 50% of the CTCs ranged from 14.5 to 18 µm. The WBCs' diameters were 11.8 ± 0.54 µm; 50% of the WBCs were within 10.5–14 µm diameter. The size distribution of WBCs and CTCs present P values less than 0.0001. However, it is noteworthy that the size distributions of CTCs and WBCs overlapped.

Additionally, it is notable that while most of the CTCs isolated using the acoustic separation device were single cells, we also identified several CTCs that were present as clusters of 2–3 cells (**Figure 7**A). Although clustered CTCs were even rarer when compared to single CTCs, CTC clusters may be of greater relevance than single CTCs for improving our understating of the mechanisms of metastasis.[41,42] Further studies on clustered CTCs could be valuable to identifying CTC subgroups and CTC cells, and may reveal important information about the metastatic process.[42–45]

Finally, the immunostaining identified some cells with both cytokeratin and leukocyte markers, namely CK8,18+ and CD45+. Although these "double-positive" cells are typically excluded from CTC enumeration, they might be inherently related to CTCs.[20] In addition, these double-positive cells are observed rarely in healthy donors' blood samples. The identity of these double-positive cells is currently not well understood. These CTCs may be "disguised" upon ingestion of leukocyte-derived proteins, while some monocytes may be coated with tumor-derived markers. To address this situation, further studies such as using other specific markers need to be performed with our acoustic separation platform. Our study shows that the double-positive cells are present in two categories: clusters with other CTCs (Figure 7B) and as individual cells (Figure 7C). The presence of cell clusters with CTCs and dual-positive cells suggests that cell-to-cell interactions are a possible mechanism for the formation of these dual-positive cells.
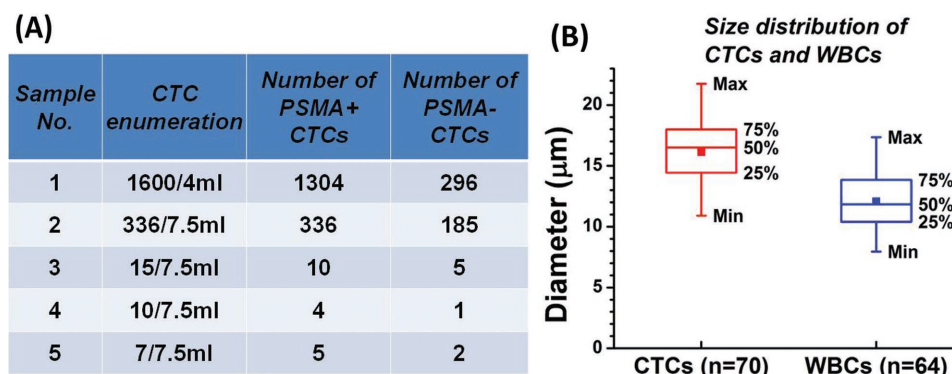
(A)

Sample No.	CTC enumeration	Number of PSMA+ CTCs	Number of PSMA- CTCs
1	1600/4ml	1304	296
2	336/7.5ml	336	185
3	15/7.5ml	10	5
4	10/7.5ml	4	1
5	7/7.5ml	5	2

(B)

Figure 6. A) The total number of CTCs collected and the PSMA expression of those CTCs from prostate cancer patients. CTCs are defined as nucleated, cytokeratin-positive, CD45-negative cells. B) The size distribution of CTCs and WBCs. The diameters of cells were calculated from images. The data were obtained from 70 CTCs and 64 WBCs all from one patient. The square dot is the average value, whereas the lined box indicates the median value (50%) as well as the 25% and 75% values of the size distribution. The minimum and maximum values are indicated as Min and Max, respectively.
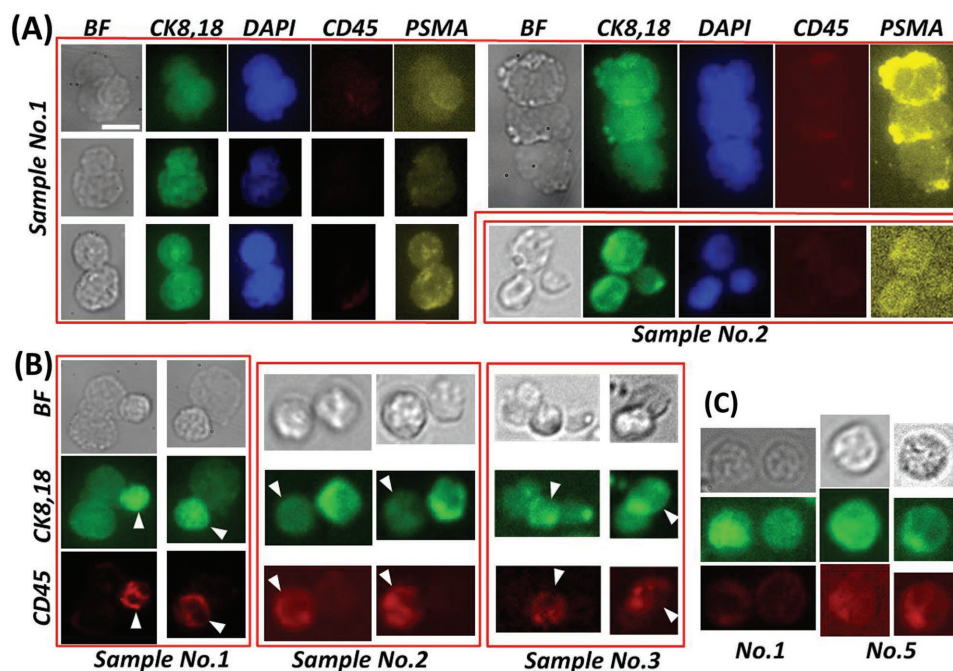
ADVANCED
SCIENCE NEWS
www.advancedsciencenews.com

NANO · MICRO
small
www.small-journal.com

Figure 7. CTC clusters and dual-positive cells are separated by the acoustic devices. A) Immunostaining images of clustered CTCs. B) Cell clusters with both CTCs (CK8,18+ and CD45−) and dual-expression cells (CK8,18+ and CD45+). C) Individual cells with dual expression of CK8,18 and CD45.

3. Discussion

We have successfully developed and tested a high-throughput, acoustic-based CTC-separation device. This device has features specifically designed to increase the acoustic energy density by using a hybrid PDMS–glass channel, and with a localized decrease in the flow velocity of cells by introducing a divider design. The ability to perform high-throughput CTC separation allows acoustic-based separation to perform tasks that were not possible with previous designs including ex vivo CTC growth studies and CTC phenotypic studies. This method can thus be developed further into a clinically useful platform for rapid, noninvasive, CTC-based biomarker studies in oncology. We isolated cancer cells from a spiked solution of WBCs at a throughput of 7.5 mL h^{-1}, and further demonstrated the successful isolation and phenotypic characterization of CTCs from clinical patient samples from men with metastatic prostate cancer. Single CTCs and clusters of CTCs were isolated and then identified by immunostaining. Their size distributions and biomarker heterogeneity profiles were statistically analyzed in order to provide proof-of-principle data on downstream analysis of CTCs in the clinic. The present method thus achieves three key characteristics simultaneously compared to prior acoustic separation designs: separation accuracy, preservation of cell integrity, and increase in throughput.

With its biocompatibility, this method opens opportunities for in vitro, downstream culturing of CTCs. Currently, only a few successful cases have been reported for in vitro culturing of CTCs, all under stringent experimental conditions and very limited CTC types, with a very low culture success rate.[45–47] One possible explanation of such limited success is that the functions and properties of CTCs were altered during the separation

and enrichment processes. In addition, positive selection for EpCAM positive cells may reduce the ability of CTCs to be cultured ex vivo, as only stem-like dedifferentiated CTCs may propagate in culture conditions.[39–47] The method developed in our work features biocompatibility without positive selection conditions, which maximizes the chances of maintaining a wide range of CTCs in their native states. We have observed the normal proliferation of cells after acoustic separation. Future work could include drug efficacy assays once the conditions suitable to grow CTCs are fully determined. This will aid in the development of targeted cancer therapies, furthering the promise of precision medicine.

With the ability to simultaneously identify, sort, and isolate CTCs in a high-throughput manner, we could investigate other unique characteristics of CTCs including phenotypic and genotypic heterogeneity. This platform permits further insight into topics such as CTC microclusters, CTC heterogeneity, and dynamic changes of CTCs. For example, we have demonstrated heterogeneity of PSMA expression in CTCs in men with metastatic castration-resistant prostate cancer (mCRPC), which has implications for PSMA-targeted imaging or therapeutics. PSMA heterogeneity in CTCs has been reported previously in the context of androgen receptor signaling, and our work validates and extends these findings. Heterogeneity for a range of differentiation biomarkers has been well described in prostate cancer, suggesting that epithelial plasticity or clonal evolution strongly contributes to the diversity of CTC phenotypes.[46,48] Together, this work suggests that acoustics based CTC isolation may facilitate improved understanding of cancer metastasis mechanisms in patients over time.[40] For example, it is still unclear which genetic or epigenetic mechanisms enable CTCs to survive in the circulation, cluster, or constitute microemboli within

ADVANCED
SCIENCE NEWS

www.advancedsciencenews.com

NANO · MICRO

small

www.small-journal.com

capillary beds,[41,42,49] altering their phenotype and causing them to survive in blood circulation and distant organs. The present work could provide a tool to conduct further studies on CTCs that could help rationalize the metastatic cascade for therapeutic interventions.

In this work, all the RBCs are removed using a RBC lysis buffer before the CTC isolation process. Other CTC isolation methods have also utilized RBC lysis buffers prior to CTC isolation and reported no significant damage to isolated cancer cells.[42,50] However, the RBC lysis step requires extra sample processing time and may lead to considerable loss of cancer cells or WBCs, or may alter the properties of the CTCs. In this regard, it is desirable for future studies to integrate a RBC-removal function into the same acoustic separation chip. Since the acoustofluidic method isolates cells based on differences in size or other physical properties, acoustic separation of RBCs (diameter ≈7 µm, thickness ≈3 µm) and WBCs (diameter ≈12 µm) should be achievable. This will inevitably call for steps to address issues such as maintaining separation efficiency in highly viscous fluids such as undiluted whole blood. The present method also offers potential other applications, such as blood component separation, cell washing, and bacteria separation.[51,52]

4. Experimental Section

Device Fabrication: In this study, Y+128° X-propagation lithium niobate (LiNbO₃) was used as piezoelectric substrate. The IDT design was patterned by photolithography using a MA/BA6 mask aligner (SUSS MicroTec., Germany). After that, 50 Å of Cr was deposited as an adhesive layer, followed by a 500 Å gold layer for electrode fabrication. The deposition was conducted with an e-beam evaporator (Semicore Corp, USA). Finally, the metal layer was removed with photoresist and IDTs were formed by a lift-off process.

The PDMS/glass hybrid channel was fabricated by a standard soft lithography process, as shown in Figure S1 (Supporting Information). A thin layer of SU8 100 photoresist (MicroChem, USA) was spin-coated and patterned by ultraviolet (UV) exposure on a silicon wafer. A glass slide was placed on the SU8 mold at the designed position where standing acoustic filed was formed. The glass slide was made from micro cover glass (VWR, USA), and was cut to 800 µm × 5 mm by laser cutting. Sylgard 184 Silicone Elastomer Curing Agent and Base (Dow Corning, USA) were mixed at 1:10 and poured on the mold. After setting at room temperature overnight, the PDMS channel was peeled from the mold and bonded to the LiNbO₃ substrate. Before bonding, the surface of the LiNbO₃ substrate and the PDMS channel were treated with oxygen plasma.

Experimental Setup and Procedures: The high-throughput acoustic separation device was placed on a Peltier cooler (TEC1-12730, Hebei I.T., China), which served as a heat sink. The voltage for the cooler was ≈2 V. The device and cooler were placed on the stage of an upright microscope (BX51WI, Olympus, Japan) during the separation experiment. The fluid flows, including sheath fluid and sample fluid, were controlled by individual syringe pumps (neMESYS, cetoni GmbH, Germany). Before each experiment, ethanol was flushed through the whole microfluidic device to remove air bubbles from the channel, followed by PBS washing for 3 min. Then the channel was filled with 1% bovine serum albumin (Sigma-Aldrich, USA) solution and left for 5 min to coat the channel surface. The sample mixture was then introduced to the device at a flow rate of 125 µL min⁻¹. The flow rates for two sheath fluids were 110 and 220 µL min⁻¹. Cells from the device outlets were collected either in a 35 × 10 mm² Petri dish (Corning) or 1.7 mL Eppendorf centrifuge tubes. The acoustic wave was excited by applying a radio frequency (RF) signal to the IDTs on the piezoelectric substrate. The RF signal was generated by a function generator (E4422B; Agilent, USA) and an

amplifier (25A100A; Amplifier Research, USA). The frequency was set at 19.9 MHz, and the power inputs ranged from 32 to 35 dBm.

Cell Cultures and Sample Preparation: MCF-7 (HTB-22), HeLa (CCL-2) cells, PC-3, and LNCaP cells were purchased from ATCC. MCF-7 cells were cultured using Earle's minimum essential medium (Cellgro; Corning, USA) supplemented with 10% (vol/vol) fetal bovine serum (FBS) solution (Atlanta Biologicals) and 1% penicillin–streptomycin solution (Mediatech Inc., USA). HeLa, PC-3, and LNCaP cells were cultured with DMEM/Ham's F-12 50/50 Mix (Life Technologies, USA) supplemented with 10% (vol/vol) FBS and 1% penicillin–streptomycin solution. All of the cell lines were maintained in an incubator (NU-4750; NuAire, UK) at a temperature of 37 °C and 5% CO₂ level. Before each experiment, cells were detached from the surface of culture flasks with 0.05% trypsin (Cellgro; Corning, USA). The resulting cell suspensions were then centrifuged at 800 rpm and resuspended with 1 × PBS buffer. To label cells with Calcein-AM (Invitrogen, USA), cells were incubated with 1 × 10⁻⁶ M Calcein-AM in 1 × PBS solution at room temperature for 15 min. Cells were washed by spinning down at 800 rpm and resuspending into a new portion of PBS solution. To prepare WBCs, human whole blood (Zen-Bio, USA) was lysed with RBC lysis buffer (eBioscience, Thermo Fisher Scientific, USA) at a volume ratio of 1:10. The mixture solution was incubated for 5–10 min at room temperature and then centrifuged at 800 g. The supernatant was removed and the cell pellet was resuspended using PBS. For long-term storage, WBCs were fixed using 4% (wt/vol) paraformaldehyde (Santa Cruz Biotechnology, USA) at room temperature for 30 min.

Patients' Blood Processing, Immunofluorescence Staining, and Image Acquisition: Men with mCRPC and progressive bone metastases were consented to a Duke IRB approved clinical protocol permitting CTC isolation and characterization. Whole blood samples were collected in 7.5 mL ethylenediaminetetraacetic acid (EDTA) tubes and used within 24 h after collection. Red blood cells in the collected samples were then lysed by a 5 min treatment of RBC lysis buffer, followed by centrifugation at 800 g. After removing the supernatant, WBCs and CTCs were collected and resuspended in 7.5 mL of PBS solution with 0.1% PF-68. The mixture was then injected through the high-throughput acoustic separation device. The flow rate of sample was set as 7.5 mL h⁻¹. The isolated sample was collected from the outlet and concentrated via centrifugation to 1 mL for immunofluorescence staining.

To perform staining, cells were first fixed by 4% (wt/vol) paraformaldehyde (Santa Cruz Biotechnology, USA) for 10 min. Then, cells were treated by 0.1% Triton X-100 (Sigma, USA) in PBS solution for 10 min to enhance permeability and 200 µL of 3% (wt/vol) bovine serum albumin (Sigma-Aldrich, USA) in PBS solution for 30 min to block nonspecific binding sites. After that, cells were incubated in 3% (wt/vol) bovine serum albumins solution at 4 °C overnight with 5 µL fluorescein-isothiocyanate-labeled mouse anti-CK 8, 18 (Abcam, UK), 5 µL phycoerythrin-labeled anti-human PSMA (Abcam, UK), and 5 µL Cy5-labeled mouse anti-CD45 (eBioscience, Thermo Fisher Scientific, USA) added. Cells were then washed with PBS. At this time, DAPI (Sigma-Aldrich, USA) was added to the cell solution to stain cell nuclei. The cell solution was then transported to a chamber slide (8 well Lab-Tek II Chamber Slide, ThermoFisher Scientific, USA) for observation using an inverted fluorescence microscope (Ti-U Eclipse; Nikon, Japan) and a charge-coupled device (CCD) camera (CoolSNAP HQ2; Photometrics, USA). The images were processed and analyzed using ImageJ (NIH, USA).

Supporting Information

Supporting Information is available from the Wiley Online Library or from the author.

Acknowledgements

Conflict of Interest

The authors declare no conflict of interest.

Keywords

[1] V. Plaks, C. Koopman, Z. Werb, *Science* **2013**, *341*, 1186.
[2] C. Alix-Panabieres, K. Pantel, *Clin. Chem.* **2013**, *59*, 110.
[3] M. Cristofanilli, *Semin. Oncol.* **2006**, *33*, 9.
[4] M. Cristofanilli, D. Hayes, G. Budd, M. Ellis, A. Stopeck, J. Reuben, G. Doyle, J. Matera, W. Allard, M. Miller, H. Fritsche, G. Hortobagyi, L. Terstappen, *J. Clin. Oncol.* **2005**, *23*, 1420.
[5] D. Danila, G. Heller, G. Gignac, R. Gonzalez-Espinoza, A. Anand, E. Tanaka, H. Lilja, L. Schwartz, S. Larson, M. Fleisher, H. Scher, *Clin. Cancer Res.* **2007**, *13*, 7053.
[6] J. de Bono, H. Scher, R. Montgomery, C. Parker, M. Miller, H. Tissing, G. Doyle, L. Terstappen, K. Pienta, D. Raghavan, *Clin. Cancer Res.* **2008**, *14*, 6302.
[7] J. Smerage, W. Barlow, G. Hortobagyi, E. Winer, B. Leyland-Jones, G. Srkalovic, S. Tejwani, A. Schott, M. O'Rourke, D. Lew, G. Doyle, J. Gralow, R. Livingston, D. Hayes, *J. Clin. Oncol.* **2014**, *32*, 3483.
[8] M. Ignatiadis, M. Reinholz, *Breast Cancer Res.* **2011**, *13*, 222.
[9] E. Antonarakis, C. Lu, H. Wang, B. Luber, M. Nakazawa, J. Roeser, Y. Chen, T. Mohammad, Y. Chen, H. Fedor, T. Lotan, Q. Zheng, A. De Marzo, J. Isaacs, W. Isaacs, R. Nadal, C. Paller, S. Denmeade, M. Carducci, M. Eisenberger, J. Luo, *N. Engl. J. Med.* **2014**, *371*, 1028.
[10] S. Gupta, J. Li, G. Kemeny, R. Bitting, J. Beaver, J. Somarelli, K. Ware, S. Gregory, A. Armstrong, *Clin. Cancer Res.* **2017**, *23*, 1346.
[11] W. Abida, H. Scher, *JAMA Oncol.* **2017**, *3*, 1673.
[12] S. Maheswaran, D. Haber, *Curr. Opin. Genet. Dev.* **2010**, *20*, 96.
[13] M. Al-Hajj, M. Wicha, A. Benito-Hernandez, S. Morrison, M. Clarke, *Proc. Natl. Acad. Sci. USA* **2003**, *100*, 3983.
[14] J. Lohr, V. Adalsteinsson, K. Cibulskis, A. Choudhury, M. Rosenberg, P. Cruz-Gordillo, J. Francis, C. Zhang, A. Shalek, R. Satija, J. Trombetta, D. Lu, N. Tallapragada, N. Tahirova, S. Kim, B. Blumenstiel, C. Sougnez, A. Lowe, B. Wong, D. Auclair, E. Van Allen, M. Nakabayashi, R. Lis, G. Lee, T. Li, M. Chabot, A. Ly, M. Taplin, T. Clancy, M. Loda, A. Regev, M. Meyerson, W. Hahn, P. Kantoff, T. Golub, G. Getz, J. Boehm, J. Love, *Nat. Biotechnol.* **2014**, *32*, 479.
[15] Y. Kang, P. Siegel, W. Shu, M. Drobnjak, S. Kakonen, C. Cordón-Cardo, T. Guise, J. Massagué, *Cancer Cell* **2003**, *3*, 537.
[16] A. Minn, G. Gupta, D. Padua, P. Bos, D. Nguyen, D. Nuyten, B. Kreike, Y. Zhang, Y. Wang, H. Ishwaran, J. Foekens, M. van de Vijver, J. Massague, *Proc. Natl. Acad. Sci. USA* **2007**, *104*, 6740.
[17] A. van de Stolpe, K. Pantel, S. Sleijfer, L. Terstappen, J. den Toonder, *Cancer Res.* **2011**, *71*, 5955.
[18] A. Barradas, L. Terstappen, *Cancers* **2013**, *5*, 1619.
[19] S. Nagrath, L. Sequist, S. Maheswaran, D. Bell, D. Irimia, L. Ulkus, M. Smith, E. Kwak, S. Digumarthy, A. Muzikansky, P. Ryan, U. Balis, R. Tompkins, D. Haber, M. Toner, *Nature* **2007**, *450*, 1235.
[20] W. Wang, H. Cui, P. Zhang, J. Meng, F. Zhang, S. Wang, *ACS Appl. Mater. Interfaces* **2017**, *9*, 10537.
[21] S. Hou, H. Zhao, L. Zhao, Q. Shen, K. Wei, D. Suh, A. Nakao, M. Garcia, M. Song, T. Lee, B. Xiong, S. Luo, H. Tseng, H. Yu, *Adv. Mater.* **2013**, *25*, 1547.
[22] Y. Li, Q. Lu, H. Liu, J. Wang, P. Zhang, H. Liang, L. Jiang, S. Wang, *Adv. Mater.* **2015**, *27*, 6848.
[23] A. Talasaz, A. Powell, D. Huber, J. Berbee, K. Roh, W. Yu, W. Xiao, M. Davis, R. Pease, M. Mindrinos, S. Jeffrey, R. Davis, *Proc. Natl. Acad. Sci. USA* **2009**, *106*, 3970.
[24] E. Ozkumur, A. Shah, J. Ciciliano, B. Emmink, D. Miyamoto, E. Brachtel, M. Yu, P. Chen, B. Morgan, J. Trautwein, A. Kimura, S. Sengupta, S. Stott, N. Karabacak, T. Barber, J. Walsh, K. Smith, P. Spuhler, J. Sullivan, R. Lee, D. Ting, X. Luo, A. Shaw, A. Bardia, L. Sequist, D. Louis, S. Maheswaran, R. Kapur, D. Haber, M. Toner, *Sci. Transl. Med.* **2013**, *5*, 179ra47.
[25] M. Warkiani, B. Khoo, D. Tan, A. Bhagat, W. Lim, Y. Yap, S. Lee, R. Soo, J. Han, C. Lim, *The Analyst* **2014**, *139*, 3245.
[26] M. Warkiani, B. Khoo, L. Wu, A. Tay, A. Bhagat, J. Han, C. Lim, *Nat. Protoc.* **2015**, *11*, 134.
[27] H. Moon, K. Kwon, S. Kim, H. Han, J. Sohn, S. Lee, H. Jung, *Lab Chip* **2011**, *11*, 1118.
[28] S. Shim, K. Stemke-Hale, A. Tsimberidou, J. Noshari, T. Anderson, P. Gascoyne, *Biomicrofluidics* **2013**, *7*, 011807.
[29] P. Li, Z. Mao, Z. Peng, L. Zhou, Y. Chen, P. Huang, C. Truica, J. Drabick, W. El-Deiry, M. Dao, S. Suresh, T. Huang, *Proc. Natl. Acad. Sci. USA* **2015**, *112*, 4970.
[30] Y. Chen, M. Wu, L. Ren, J. Liu, P. Whitley, L. Wang, T. Huang, *Lab Chip* **2016**, *16*, 3466.
[31] S. Li, F. Ma, H. Bachman, C. Cameron, X. Zeng, T. Huang, *J. Micromech. Microeng.* **2017**, *27*, 015031.
[32] M. Wu, Y. Ouyang, Z. Wang, R. Zhang, P. Huang, C. Chen, H. Li, P. Li, D. Quinn, M. Dao, S. Suresh, Y. Sadovsky, T. Huang, *Proc. Natl. Acad. Sci. USA* **2017**, *114*, 201709210.
[33] T. Hasegawa, K. Yosioka, *J. Acoust. Soc. Am.* **1969**, *46*, 1139.
[34] X. Ding, Z. Peng, S. Lin, M. Geri, S. Li, P. Li, Y. Chen, M. Dao, S. Suresh, T. Huang, *Proc. Natl. Acad. Sci. USA* **2014**, *111*, 12992.
[35] R. Sellin, *Flow in Channels*, Macmillan, London **1969**.
[36] R. Lapidus, C. Tiffany, J. Isaacs, B. Slusher, *Prostate* **2000**, *45*, 350.
[37] A. Ghosh, W. Heston, *J. Cell. Biochem.* **2004**, *91*, 528.
[38] C. Zechmann, A. Afshar-Oromieh, T. Armor, J. Stubbs, W. Mier, B. Hadaschik, J. Joyal, K. Kopka, J. Debus, J. Babich, U. Haberkorn, *Eur. J. Nucl. Med. Mol. Imaging* **2014**, *41*, 1280.
[39] X. Wu, B. Ding, J. Gao, H. Wang, W. Fan, X. Wang, W. Zhang, X. Wang, L. Ye, M. Zhang, X. Ding, J. Liu, Q. Zhu, S. Gao, *Int. J. Nanomed.* **2011**, *6*, 1747.
[40] D. Miyamoto, R. Lee, S. Stott, D. Ting, B. Wittner, M. Ulman, M. Smas, J. Lord, B. Brannigan, J. Trautwein, N. Bander, C. Wu, L. Sequist, M. Smith, S. Ramaswamy, M. Toner, S. Maheswaran, D. Haber, *Cancer Discovery* **2012**, *2*, 995.
[41] N. Aceto, A. Bardia, D. Miyamoto, M. Donaldson, B. Wittner, J. Spencer, M. Yu, A. Pely, A. Engstrom, H. Zhu, B. Brannigan, R. Kapur, S. Stott, T. Shioda, S. Ramaswamy, D. Ting, C. Lin, M. Toner, D. Haber, S. Maheswaran, *Cell* **2014**, *158*, 1110.
[42] A. Sarioglu, N. Aceto, N. Kojic, M. Donaldson, M. Zeinali, B. Hamza, A. Engstrom, H. Zhu, T. Sundaresan, D. Miyamoto, X. Luo, A. Bardia, B. Wittner, S. Ramaswamy, T. Shioda, D. Ting, S. Stott, R. Kapur, S. Maheswaran, D. Haber, M. Toner, *Nat. Methods* **2015**, *12*, 685.

[43] J. Hou, M. Krebs, L. Lancashire, R. Sloane, A. Backen, R. Swain, L. Priest, A. Greystoke, C. Zhou, K. Morris, T. Ward, F. Blackhall, C. Dive, *J. Clin. Oncol.* **2012**, *30*, 525.

[44] P. Theodoropoulos, H. Polioudaki, S. Agelaki, G. Kallergi, Z. Saridaki, D. Mavroudis, V. Georgoulias, *Cancer Lett.* **2010**, *288*, 99.

[45] I. Baccelli, A. Schneeweiss, S. Riethdorf, A. Stenzinger, A. Schillert, V. Vogel, C. Klein, M. Saini, T. Bäuerle, M. Wallwiener, T. Holland-Letz, T. Höfner, M. Sprick, M. Scharpff, F. Marmé, H. Sinn, K. Pantel, W. Weichert, A. Trumpp, *Nat. Biotechnol.* **2013**, *31*, 539.

[46] M. Yu, A. Bardia, N. Aceto, F. Bersani, M. Madden, M. Donaldson, R. Desai, H. Zhu, V. Comaills, Z. Zheng, B. Wittner, P. Stojanov, E. Brachtel, D. Sgroi, R. Kapur, T. Shioda, D. Ting, S. Ramaswamy, G. Getz, A. Iafrate, C. Benes, M. Toner, S. Maheswaran, D. Haber, *Science* **2014**, *345*, 216.

[47] L. Zhang, L. Ridgway, M. Wetzel, J. Ngo, W. Yin, D. Kumar, J. Goodman, M. Groves, D. Marchetti, *Sci. Transl. Med.* **2013**, *5*, 180ra48.

[48] A. Armstrong, M. Marengo, S. Oltean, G. Kemeny, R. Bitting, J. Turnbull, C. Herold, P. Marcom, D. George, M. Garcia-Blanco, *Mol. Cancer Res.* **2011**, *9*, 997.

[49] S. Au, B. Storey, J. Moore, Q. Tang, Y. Chen, S. Javaid, A. Sarioglu, R. Sullivan, M. Madden, R. O'Keefe, D. Haber, S. Maheswaran, D. Langenau, S. Stott, M. Toner, *Proc. Natl. Acad. Sci. USA* **2016**, *113*, 4947.

[50] K. Hyun, K. Kwon, H. Han, S. Kim, H. Jung, *Biosens. Bioelectron.* **2013**, *40*, 206.

[51] Y. Chen, P. Li, P. Huang, Y. Xie, J. Mai, L. Wang, N. Nguyen, T. Huang, *Lab Chip* **2014**, *14*, 626.

[52] A. Lenshof, T. Laurell, *Chem. Soc. Rev.* **2010**, *39*, 1203.